Piezo activity levels need to be tightly regulated to maintain normal morphology and function in pericardial nephrocytes

Kristina Schulz, PhD [1,2,*], Paris Hazelton-Cavill [1,2,*], Karl K. Alornyo [1,2,*], Ilka Edenhofer [1,2], Maja Lindenmeyer, PhD [1,2], Christian Lohr, PhD [4], Tobias B. Huber, MD [1,2], Barry Denholm, PhD [3] and Sybille Koehler, PhD [1,2,3]

[1] III. Department of Medicine, University Medical Center Hamburg-Eppendorf, Hamburg, Germany; [2] Hamburg Center for Kidney Health (HCKH), University Medical Center Hamburg-Eppendorf, Hamburg, Germany; [3] Biomedical Sciences, University of Edinburgh, Edinburgh, Scotland, UK; [4] Division of Neurophysiology, Institute of Cell and Systems Biology of Animals, University of Hamburg, Hamburg, Germany

*Contributed equally

Corresponding author:

Sybille Koehler

Campus Forschung N27
Martinistraße 52
UKE Hamburg
20246 Hamburg
Germany

Sy.koehler@uke.de

Abstract

Due to their position on glomerular capillaries, podocytes are continuously counteracting biomechanical filtration forces. Most therapeutic interventions known to generally slow or prevent the progression of chronic kidney disease appear to lower these biomechanical forces on podocytes, highlighting the critical need to better understand podocyte mechano-signalling pathways. Here we investigated whether the mechanotransducer Piezo is involved in a mechanosensation pathway in *Drosophila* nephrocytes, the podocyte homologue in the fly.

Loss of function analysis in Piezo depleted nephrocytes reveal a severe morphological and functional phenotype. Further, pharmacological activation of endogenous Piezo with Yoda1 causes a significant increase of intracellular Ca^{++} upon exposure to a mechanical stimulus in nephrocytes, as well as filtration disturbances. Elevated Piezo expression levels also result in a severe nephrocyte phenotype. Interestingly, expression of Piezo which lacks mechanosensitive channel activity, does not result in a severe nephrocyte phenotype, suggesting the observed changes in Piezo wildtype overexpressing cells are caused by the mechanosensitive channel activity. Moreover, blocking Piezo activity using the tarantula toxin GsMTx4 reverses the phenotypes observed in nephrocytes overexpressing Piezo.

Taken together, here we provide evidence that Piezo activity levels need to be tightly regulated to maintain normal pericardial nephrocyte morphology and function.

72 **Introduction**

73 Kidney podocytes are highly specialized epithelial cells, which together with the
74 fenestrated endothelium and the glomerular basement membrane, constitute the
75 three-layered, size and charge selective filter of the glomerular filtration barrier [1].
76 Podocytes have a unique morphology, forming primary and secondary foot processes
77 which completely enwrap the capillaries. Injury to podocytes causes severe
78 morphological change, detachment from the basement membrane and finally loss of
79 podocytes into the primary urine with pathological consequences as these cells are
80 post-mitotic and cannot be replenished. Podocyte injury can occur because of a variety
81 of mechanisms, among them genetic deficiencies [2–6], toxin-mediated triggers [7] and
82 changes in the physical environment within the glomerulus [8–11].

83 Podocytes are under constant mechanical force and regularly face changes in
84 these forces, as they are responsible for the filtration of ~180 litres of primary urine
85 each day. The main forces arising from this are hydrostatic pressure (50 kPa) and fluid
86 shear stress at the filtration slits (8 Pa) [12]. These forces increase during diseases such
87 as diabetes and hypertension and result in podocyte loss [10]. It has previously been
88 shown, that increased biomechanical force such as glomerular hypertension and fluid
89 shear stress can cause podocyte depletion [13–15]. Further, it is known, that remaining
90 podocytes respond by growing in size to re-cover the blank capillary to overcome the
91 challenge originating from loss of neighbouring cells; this is considered to be an
92 adaptive and protective mechanism [14,16,17]. In order for this to happen, one possible
93 hypothesis is that podocytes exhibit mechanotransductive mechanisms to recognize
94 these changes in the physical environment and initiate adaptive and protective
95 responses, likely candidates are TRPC6, YAP, Talin, Filamins and Piezo [5,8,9,18–21].

96 Piezo is a mechanosensitive ion channel that is involved in
97 mechanotransduction in many developmental and physiological contexts. Piezo

channels (Piezo1 and Piezo2) open in response to mechanical force/stimuli and allow the influx of positively charged ions such as Ca^{++} and Na^{+} [22,23]. The two proteins have different functional roles as Piezo1 was reported to be essential for sensing blood flow-associated shear stress and blood vessel development [24–26], while Piezo2 responds to touch and proprioception [27].

Whether Piezo plays a role in mechanotransduction in nephrocytes, the podocyte homologue in flies, is unknown. To address this question, we investigated the effect of Piezo depletion, activation and overexpression on nephrocyte morphology and function. Nephrocytes form foot processes, which are spanned by the nephrocyte diaphragm, a highly-specialized cell-cell contact, that is highly similar to the mammalian filtration barrier in the glomeruli [28,29]. They function as filtration units in the fly and filter toxins and waste products from the haemolymph. Our data show that Piezo functions as a mechanotransducer in nephrocytes and reveal the need for careful regulation of its expression levels to prevent a nephrocyte phenotype.

124 **Results**

125 **Piezo1 is expressed in mammalian podocytes**

126 To investigate the functional role of Piezo we utilized *Drosophila* nephrocytes,
127 the homologue cells to mammalian podocytes. To confirm Piezo expression in
128 nephrocytes, we analysed publicly available single nucleus RNAsequencing data from
129 the fly kidney atlas, which shows expression of Piezo in garland nephrocytes (36.6%
130 of cells) and pericardial cells (18.3% of cells) [30]. Of note, in *Drosophila* only one Piezo
131 isoform is present, with equal similarity to human Piezo1 and Piezo2. As Piezo specific
132 antibodies for Drosophila are elusive, we decided to confirm the presence of the
133 channel by loss of function analysis and using a specific activator of the channel
134 combined with assessment of downstream signaling pathways.

135 However, we examined Piezo1 protein expression in mammalian tissue.
136 Proteomic analysis of isolated murine podocytes revealed expression of Piezo1
137 (12.25% enrichment when compared to non-podocyte glomerular cells) [31],
138 strengthening support for our hypothesis that Piezo1 is a mechanotransducer in
139 mammalian podocytes as well. Moreover, recent studies confirmed expression of
140 Piezo1 in podocytes and also showed increased Piezo1 expression in podocytes in
141 experimental hypertensive nephropathy and lupus nephritis [32,33]. We examined
142 expression of Piezo1 in mammalian glomeruli, by co-staining with the podocyte marker
143 Synaptopodin and found Piezo1 expression in podocytes **(Figure 1A)**. Of note Piezo1
144 seems to localize within foot processes as co-localisation with synaptopodin was
145 observed, but also within the cell body. Investigating publicly available single nucleus
146 RNAsequencing data for human kidney also revealed expression of Piezo1 in
147 podocytes, which seems to decrease in diabetic kidney disease **(Figure 1B)** [34].
148 Moreover, searching Piezo1 in the single cell RNAsequencing data from the Kidney

149 Precision Medicine Project revealed a disease-associated expression of the channel
150 (mean expression: healthy controls: 1.45; chronic kidney disease (CKD): 1.73).
151 Taken together, these data show Piezo1 is expressed in murine and human
152 podocytes, localizes within the foot processes and the cell body and seems to have a
153 disease-associated expression pattern.

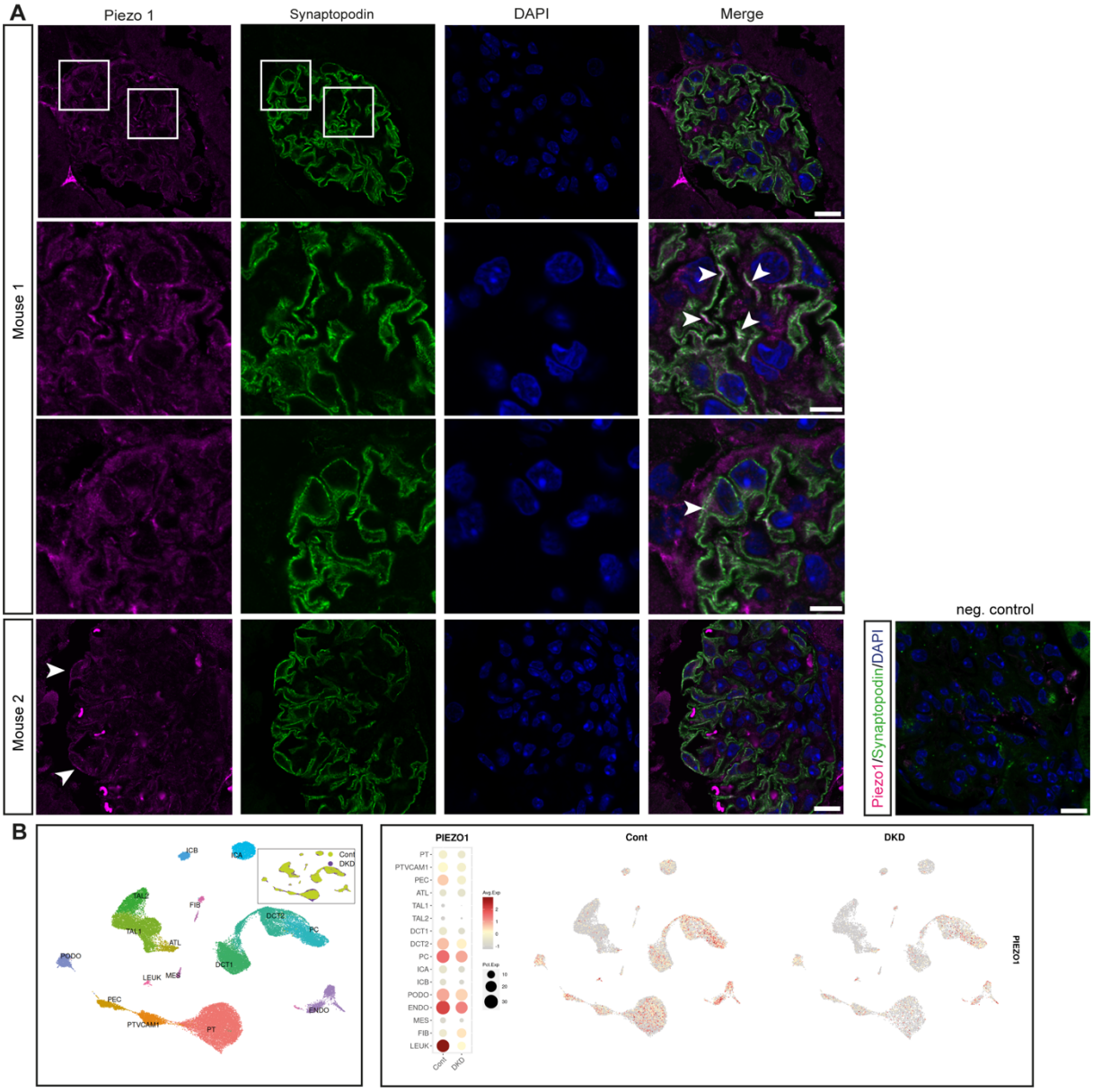

154 Figure 1

155 **Figure 1: Expression of Piezo in mammalian tissue. A** Piezo1 is expressed in mammalian podocytes,
156 which are visualized using the podocyte marker Synaptopodin. Piezo1 is expressed in areas close to
157 the slit diaphragm and in the cell body (arrow heads). Scale bar = 10μm. Negative control: without
158 primary antibodies. Scale bar = 10μm. **B** Single nucleus RNAsequencing data from human diabetic
159 kidney disease samples (DKD) and controls reveal Piezo1 expression in podocytes, which decreases
160 in DKD. Data used from the Humphries lab with permission [34]. PT: proximal tubule, PTVCAM1:
161 VCAM1(+) proximal tubule, PEC: parietal epithelial cells, ATL: ascending thin limb, TAL1: CLDN16(-)

thick ascending limb, Tal2: CLDN16(+) thick ascending limb, DCT1: early distal convoluted tubule, DT2: late distal convoluted tubule, PC: principal cells, ICA: type A intercalated cells, ICB: type B intercalated cells, PODO: podocytes, ENDO: endothelial cells, MES: mesangial cells and vascular smooth muscle cells, FIB: fibroblasts, LEUK: leukocytes.

Loss of Piezo results in a morphological and functional nephrocyte phenotype

Due to confirmed expression of Piezo1 in podocytes by us and others [21,32,33], we then examined its role in nephrocytes. Within this study, we mainly focused on assessment of adult pericardial nephrocytes as this cell type is attached to the heart tube, which exhibits peristaltic movements and induces haemolymph movement. Thus, one can envision that adult pericardial nephrocytes experience some kind of biomechanical force *in vivo*. To unravel whether the mechanotransducer Piezo is present in nephrocytes, and moreover, is important for nephrocyte function, we used Piezo-specific RNAi for nephrocyte-specific depletion of Piezo. Here, two temperatures have been assessed, with increasing temperature causing increased activity of the nephrocyte-specific Gal4 driver, thus higher expression of Piezo-RNAi and increased knockdown efficiency. We investigated morphology of pericardial nephrocytes by visualizing the nephrocyte diaphragm using a Duf (dNEPH) and Pyd (dZO1) antibody, which reveals a finger-print like pattern in healthy nephrocytes. This resulted in a morphological phenotype, as nephrocyte diaphragm length is significantly reduced and the finger-print like pattern is less dense when compared to controls **(Figure 2A)**. Expression of Piezo-RNAi at 28°C, which increases knockdown efficiency, also results in a significant shortening of the nephrocyte diaphragm, which is more severe in comparison to 25°C **(Figure 2B)**. In addition to nephrocyte morphology, we also assessed nephrocyte function by performing FITC-Albumin uptake assays. FITC-Albumin can be filtered through the nephrocyte diaphragm and taken up by nephrocytes and accumulates in the lacunae prior to endocytosis. Changes in nephrocyte diaphragm integrity, subsequent alterations in the lacunae channels and

190 endocytosis therefore result in altered levels of FITC-Albumin in the lacunae system.
191 In line with the morphological phenotype, we also observed a severe and significant
192 reduction of FITC-Albumin in Piezo depleted nephrocytes at 25°C and 28°C, reflecting
193 a functional defect in adult pericardial cells **(Figure 2C,D)**.

194 Taken together, our data shows that loss of Piezo results in a morphological
195 and functional phenotype in adult pericardial cells. Further, the loss of function analysis
196 also supports our hypothesis of Piezo expression in nephrocytes.

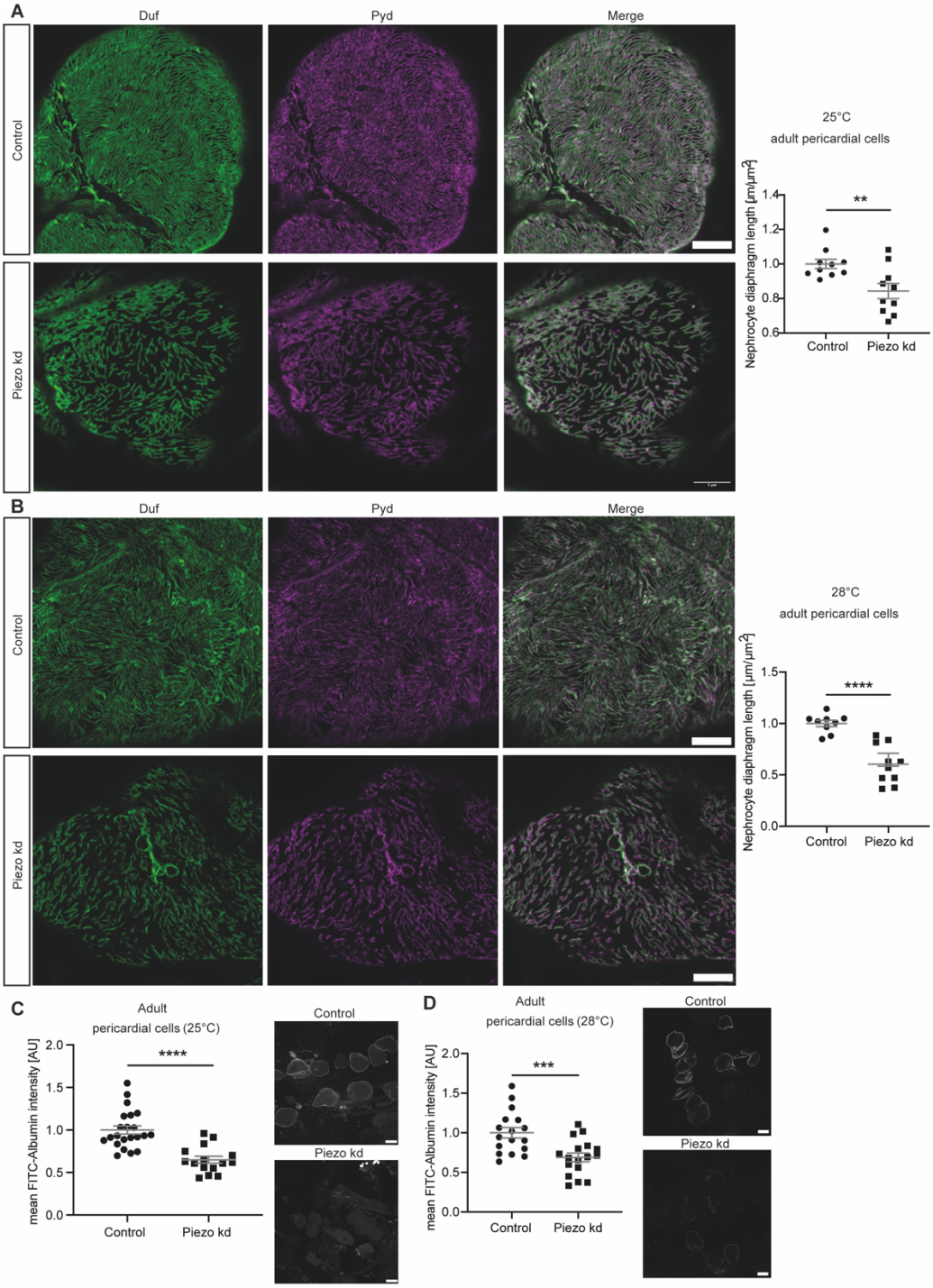

197 Figure 2

198 **Figure 2: Loss of Piezo causes a severe nephrocyte phenotype in adult pericardial cells. A**
199 Visualization of the nephrocyte diaphragm with Duf and Pyd antibodies reveals a significant decrease
200 in nephrocyte diaphragm length in adult pericardial cells upon loss of Piezo at 25°C (Piezo kd). Student's
201 t-test: **: p<0.01. Scale bar = 5µm. Control: w;*sns*-Gal4/+;+/UAS-*dicer2*; Piezo kd: w;*sns*-Gal4/+;UAS-
202 *piezo*-RNAi/UAS-*dicer2*. **B** Immunofluorescence staining with a Duf and Pyd antibody reveal significant
203 morphological changes in Piezo kd adult pericardial cells in comparison to control cells at 28°C. Scale
204 bar = 5µm. Student's t-test: ****: p<0.0001. **C** FITC-Albumin uptake assays in adult pericardial cells
205 show a significant reduction of FITC-Albumin uptake in Piezo kd cells at 25°C. Scale bar = 25µm.
206 Student's t-test: ****: p<0.0001. **D** At 28°C FITC-Albumin uptake assays show a significant filtration
207 defect in adult pericardial Piezo kd cells. Scale bar = 25µm. Student's t-test: ***: p<0.001.
208

209 **Pharmacological activation of Piezo results in an increased Ca^{++} influx and**
210 **filtration disturbances after applying a mechanical stimulus**

211 Next, we aimed to understand Piezo's role at physiological levels and when
212 exposed to mechanical stress. Hence, we pharmacologically manipulated Piezo by
213 using Yoda1, which specifically facilitates Piezo opening by reducing its mechanical
214 activation threshold [35,36]. The activation of the endogenous channel with the specific
215 activator Yoda1 will further confirm its presence in nephrocytes.

216 As Piezo is a Ca^{++} permeable cation channel and sensitive to mechanical stimuli
217 and stretch, we investigated the effect of Yoda1 by measuring Ca^{++} levels in adult
218 pericardial cells after applying a mechanical stimulus. In detail, wildtype nephrocytes
219 were incubated with either Yoda1 or the equivalent volume of DMSO and exposed to
220 a mechanical stimulus by applying a pressure-controlled puff of the corresponding
221 solution (Yoda1 or DMSO, 0.2bar for 3secs). The applied pressure stimulus (puff)
222 elicited a Ca^{++} signal in adult pericardial cells, which was significantly higher after
223 incubation in Yoda1 when compared to control conditions. This suggests that Yoda1
224 enhances the mechanosensitive channel activity of endogenous Piezo and amplifies
225 calcium signalling in these cells after applying a mechanical stimulus **(Figure 3A)**.

226 It is known that nephrocytes also elicit spontaneous calcium signals (SCSs) [37].
227 We observed similar SCSs in only 5.88% of pericardial cells, whereas 87.65% of cells
228 showed precisely timed and synchronous puff-induced calcium signals **(Supp. Figure**
229 **1A,B)**. The puff-induced signals differed significantly from SCSs in shape and timing,
230 which was confirmed by quantification of both **(Supp. Figure 1C,D,E).**

231 Moreover, Yoda1 treatment in combination with the mechanical stimulus
232 revealed a functional defect in wildtype adult pericardial cells with significantly
233 decreased FITC-Albumin accumulation **(Figure 3C)**, while morphology was unaffected
234 **(Figure 3B)**.

235 Ca^{++} has an impact on actin fibre formation, hence we investigated the actin-
236 cytoskeleton by using phalloidin, which binds to actin fibres and enables visualisation
237 of those. Although nephrocytes show an increased Ca^{++} influx in the presence of
238 Yoda1 and applying mechanical stimuli, no differences in cortical and surface actin
239 fibre formation could be observed in comparison to control cells within the time frame
240 of the experiment **(Figure 3D)**.

241 To confirm that the observed phenotypes are elicited by activation of
242 endogenous Piezo in nephrocytes through Yoda1, we performed functional
243 assessment of Piezo knockdown nephrocytes after Yoda1 treatment and application
244 of the mechanical stimulus. We assessed Ca^{++} influx in these cells, revealing that while
245 Yoda1 treated wildtype cells showed a significant increase of Ca^{++} signals after
246 applying a mechanical stimulus, this increase was significantly less in Yoda1 treated
247 Piezo knockdown cells and comparable to wildtype cells treated with DMSO **(Figure**
248 **4A)**.

249 Since the knockdown of Piezo in adult pericardial nephrocytes results in a
250 functional phenotype in the FITC-Albumin uptake assay itself, we could not assess the
251 absence of this phenotype after applying Yoda1 and a mechanical stimulus to Piezo
252 knockdown cells. Hence, we investigated Piezo loss in larval garland cells, which are
253 similar to pericardial cells, but not identical. By doing so, we did not observe a
254 functional phenotype **(Figure 4E)**. We also assessed the effects of Yoda1 treatment
255 and applying a mechanical stimulus on wildtype larval garland nephrocytes and
256 observed similar effects as in adult pericardial cells; a significant filtration defect, but
257 no difference in morphology and the actin cytoskeleton **(Figure 4B,C,D)**. Treating
258 Piezo knockdown garland nephrocytes with Yoda1 and applying a mechanical stimulus
259 did not cause significant changes in FITC-Albumin uptake, when compared to DMSO
260 treated Piezo knockdown cells or DMSO treated wildtype nephrocytes, suggesting that

261 the decreased FITC-Albumin uptake in Yoda1 treated wildtype cells is mediated by
262 Piezo **(Figure 4E)**.

263 Taken together, pharmacological activation of endogenous Piezo in
264 nephrocytes causes an increased Ca^{++} influx and a functional defect after applying
265 mechanical stimuli, while nephrocyte morphology and actin fibres were not altered
266 within the timeframe of this experiment. The observed phenotypes upon Yoda1
267 treatment and applying a mechanical stimulus can be abrogated by depleting Piezo,
268 confirming the presence and functional role of the channel in nephrocytes.

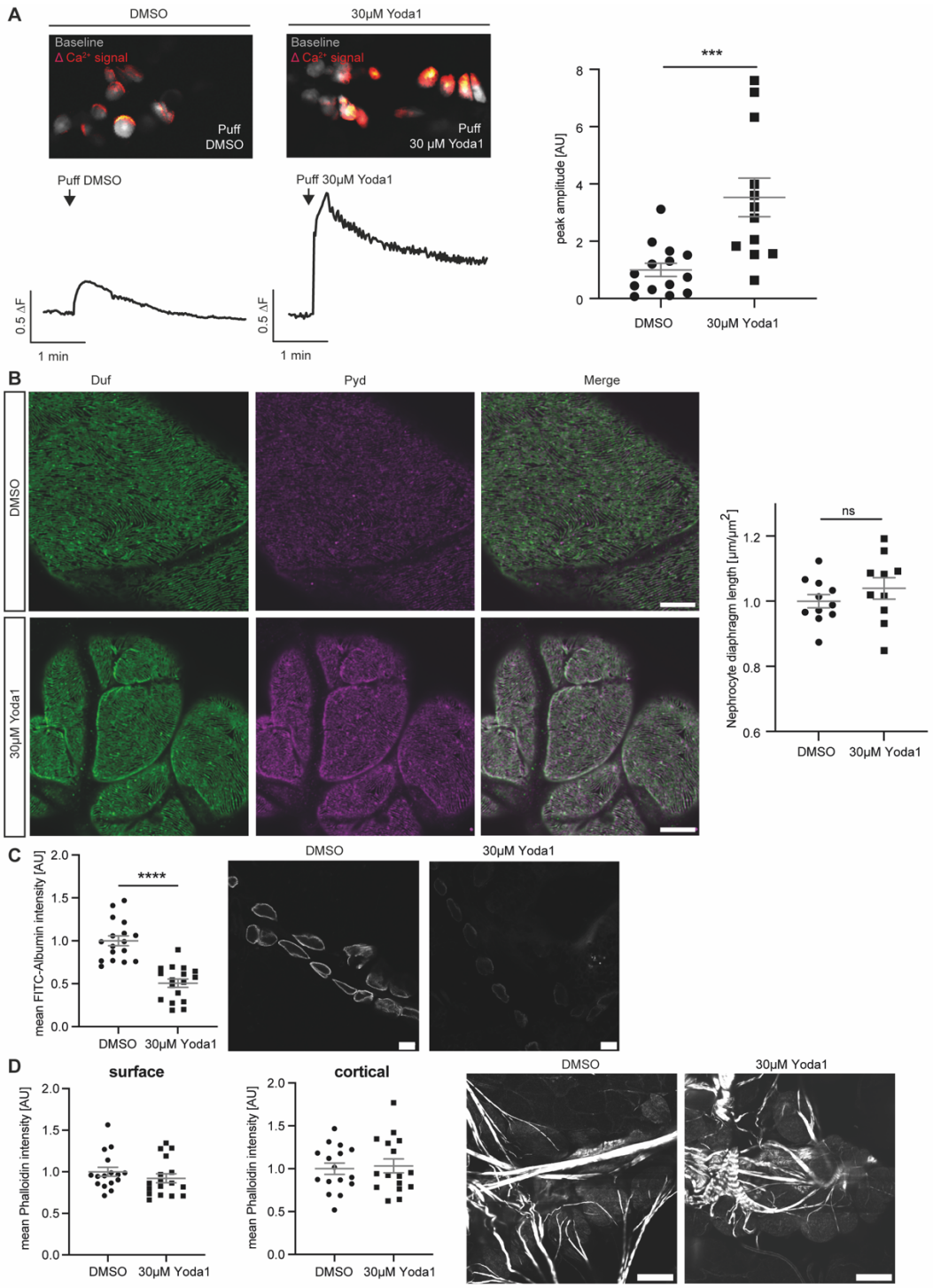

Figure 3

Figure 3: Pharmacological activation of Piezo with Yoda1 in adult pericardial nephrocytes. A Images of GCaMP6-fluorescent recordings showing puff-induced calcium signals (red) compared to baseline fluorescence (grey) in adult pericardial cells treated with DMSO (left) or 30μM Yoda1 (right). Below the images are corresponding traces of calcium signal changes over time, following a puff of DMSO (left trace) or 30μM Yoda1 (right trace). For analysis of GCamP6 intensity, ROIs of single cells have been analysed over time. Fluorescence intensity was then calculated as the mean for each fly and the maximum value within 25secs after puff is depicted as the peak amplitude. Yoda1 treated cells present with a significant increase in calcium signal amplitude after applying force (puff of Yoda1) when compared to DMSO-treated control cells (right). DMSO: 14 flies, 95 ROIs; Yoda1: 12 flies, 101 ROIs. Student's t-test: ***: $p < 0.001$. w; *sns*-Gal4/+;UAS-*dicer2*/UAS-*GCaMP6m*. **B** 5mins incubation with

Yoda1 in combination with applying a mechanical stimulus does not reveal any morphological changes as depicted by immunofluorescence staining with Duf and Pyd antibodies in adult pericardial cells. Scale bar = 5μm. **C** FITC-Albumin uptake assays reveal a significant difference between controls (DMSO) and Yoda1 treated cells, which have been exposed to a mechanical stimulus (puff). Student's t-test: ****: p < 0.0001. Scale bar = 25μm. **D** Visualisation of the actin cytoskeleton with phalloidin does not reveal any changes upon Yoda1 treatment and mechanical stimuli. Scale bar = 25μm.

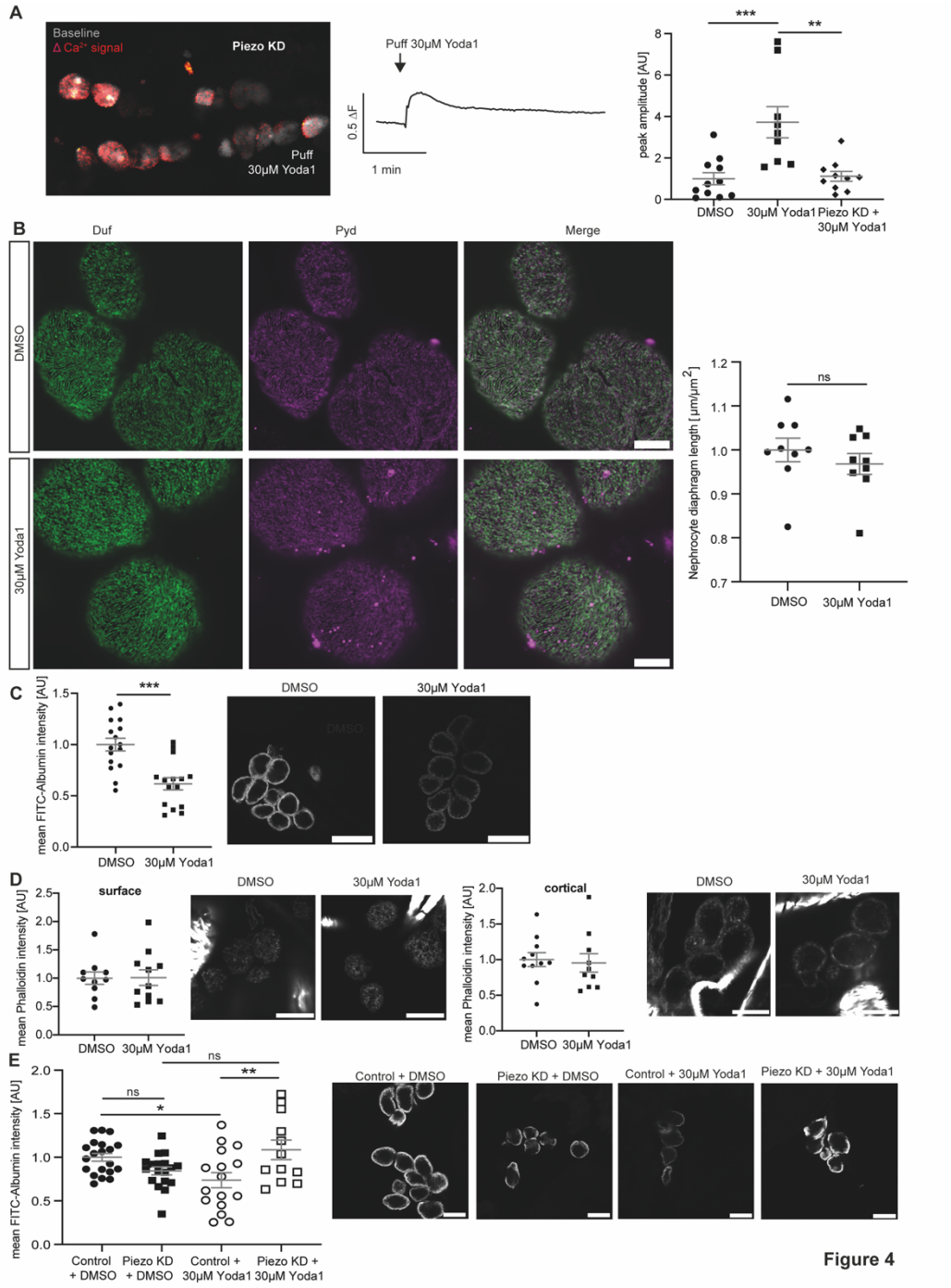

Figure 4

Figure 4: Pharmacological activation of Piezo with Yoda1 and applying mechanical force results in filtration disturbances, which are abrogated upon Piezo depletion in garland nephrocytes. A Calcium imaging reveals an abrogated calcium influx in Yoda1-treated Piezo kd pericardial cells. Images

display GCamP6-fluorescent recordings of puff-induced calcium signals (red) compared to baseline fluorescence (white) in adult pericardial cells (left). The corresponding trace shows the calcium signal over time following a puff of 30µM Yoda1 (middle). Quantification is represented as peak amplitude (right) of puff-induced calcium signals in pericardial cells from wildtype flies treated with Yoda1 (30µM), DMSO (equivalent volume) and Piezo knockdown (KD) flies treated with Yoda1 (30µM). This reveals that puff-induced calcium signals in Piezo kd cells are comparable to those in DMSO-treated wildtype cells, while Yoda1-treated wildtype cells show a significant increase in calcium signals when subjected to mechanical stress. DMSO: 11 flies, 79 ROIs; Yoda1: 9 flies, 70 ROIs; Piezo KD: 10 flies, 69 ROIs. 1way-ANOVA with Tukey's multiple comparison test: **: $p < 0.01$; ***: $p < 0.001$. **B** 5mins incubation with Yoda1 do not reveal any morphological changes as depicted by immunofluorescence staining with a Duf and Pyd antibody. Scale bar = 5µm. **C** FITC-Albumin uptake assays reveal a significant reduction of FITC-Albumin uptake after Yoda1 treatment and applying mechanical force. Scale bar = 25µm. Student's t-test: ***: $p<0.001$. **C** Visualisation of the actin cytoskeleton with phalloidin does not reveal any changes upon Yoda1 treatment and applying mechanical force. Surface and cortical levels of actin fibres have been assessed. Scale bar = 15µm (phalloidin). **D** FITC-Albumin uptake assays reveal the absence of a phenotype after Yoda1 treatment and applying mechanical force in Piezo kd nephrocytes (w;*sns*-Gal4/+;UAS-*piezo*-RNAi/UAS-*dicer2*) when compared to control cells (w;*sns*-Gal4/+;+/UAS-*dicer2*). Scale bar = 25µm. 1way-ANOVA with Tukey's multiple comparison test: *: $p < 0.05$; **: $p < 0.01$.

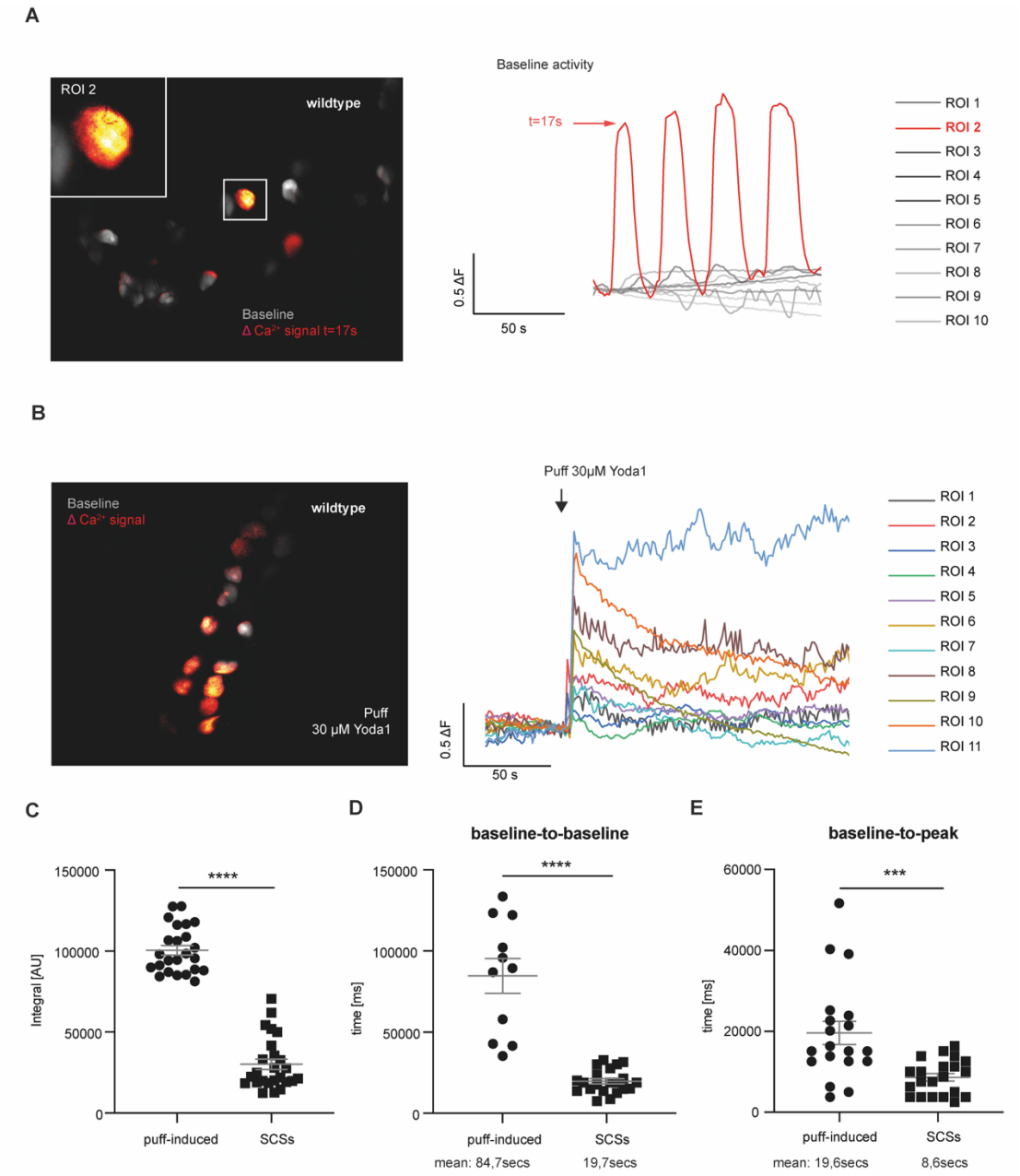

Supp. Fig. 1

Supp. Figure 1: Calcium imaging in pericardial nephrocytes. A The image (left) shows spontaneous Ca^{++} activity (red) in GCamP6 expressing nephrocytes. Each pericardial cell was marked as an ROI and changes in calcium levels over the course of an experiment are depicted in corresponding traces (right). ROI2 shows the occurrence of spontaneous calcium signals. **B** The image (left) shows synchronous puff-induced calcium signals (red) in the majority of GCamP6-expressing nephrocytes and the corresponding traces of each ROI (right). **C** Quantification of the size of the integral of puff-induced (mean of all ROIs in one fly represent a datapoint, 23 flies in total) and spontaneous calcium signals (every SCSs in 11ROIs in 9 flies).; Student's t-test: ****: $p < 0.0001$. **D** Quantification of baseline-to-baseline duration of puff-induced (mean of 11 flies, in which signals went back to baseline) and spontaneous calcium signals (every SCSs in 11ROIs in 9 flies). Student's t-test: ****: $p < 0.0001$. **E** Quantification of baseline-to-peak duration in puff-induced (mean of 19 flies) and spontaneous calcium signals (every SCSs in 11ROIs in 9 flies). Student's t-test: *** $p < 0.001$.

323 **Elevation of Piezo levels cause a nephrocyte phenotype, which is mediated by**
324 **the mechanosensitive domain**
325 Previously published data show an increase of Piezo1 levels in podocytes in a
326 hypertensive nephropathy mouse model and lupus nephritis [32,33]. Also, searching
327 publicly available human data (KPMP) revealed an increase of Piezo1 in podocytes in
328 chronic kidney disease. Hence, we further investigated whether an overexpression of
329 the channel also results in a nephrocyte phenotype. To unravel the effect of the
330 mechanosensitive domain of Piezo in nephrocytes in greater detail, we used two fly
331 strains, either expressing Piezo wildtype (Piezo WT) or a Piezo mutant lacking the
332 mechanosensitive channel activity (Piezo w/o MS) [38]. Both variants localise to the cell
333 cortex close to Pyd and within the lacunae system **(Supp. Figure 2)**. We observed a
334 morphological phenotype with decreased nephrocyte diaphragm density in adult
335 pericardial cells expressing Piezo wildtype at medium levels (25°C) **(Figure 5A; Supp.**
336 **Figure 3A)**. Interestingly, expression of the mutant lacking the mechanosensitive
337 channel activity did not cause any morphological changes at medium levels **(Figure**
338 **5A; Supp. Figure 3A)**. To assess whether a further increase of protein levels, in
339 particular of the mutant, would cause a nephrocyte phenotype, we repeated
340 morphological assessment at 28°C (high expression levels). While pericardial
341 nephrocytes expressing Piezo wildtype exhibited a significant nephrocyte phenotype,
342 expression of the mutant still did not cause any obvious changes at 28°C **(Figure 5B;**
343 **Supp. Figure 3B)**.
344 Further, we investigated nephrocyte function and observed significantly
345 decreased FITC-Albumin uptake upon expression of Piezo wildtype at 25°C and 28°C,
346 confirming a severe functional defect **(Figure 5C,D)**. We also assessed pericardial
347 nephrocytes expressing medium and high levels of the Piezo mutant regarding FITC-

348 Albumin uptake and did not observe any significant differences when compared to
349 controls **(Figure 5C,D)**.

350 Although we did not observe alterations of the actin cytoskeleton by activating
351 Piezo with Yoda1 (short-term effect), we investigated whether overexpression of Piezo
352 wildtype (long-term effect) causes changes in actin fibre formation. Visualization by
353 phalloidin and quantification of cortical actin fibres revealed a significant increase,
354 while surface levels of actin fibres are unchanged **(Figure 5E)**.

355 Taken together, overexpression of Piezo is detrimental for nephrocyte biology
356 and the observed morphological and functional phenotype seem to be mediated by its
357 mechanosensitive domain.

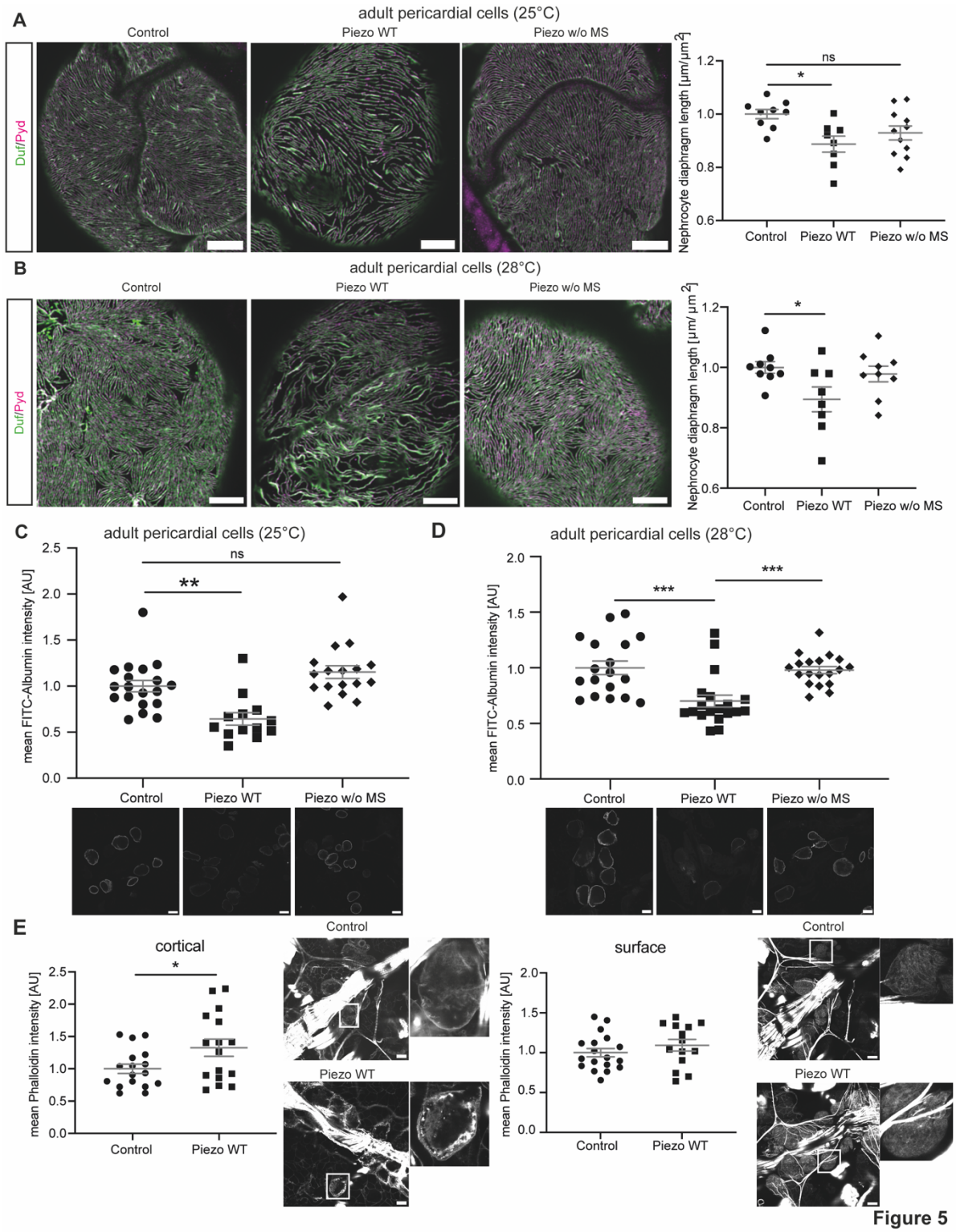

Figure 5

Figure 5: Elevated Piezo levels cause a severe nephrocyte phenotype in adult pericardial nephrocytes, which is mediated by the mechanosensitive domain. A Visualization of the nephrocyte diaphragm with Duf and Pyd antibodies shows a significant reduction of nephrocyte diaphragm length in adult pericardial cells expressing Piezo wildtype, while cells expressing the mutant without the mechanosensitive channel activity do not exhibit a phenotype. Experiments have been done at 25°C resulting in medium expression levels. Scale bar = 5µm. 1way-ANOVA with Tukey's multiple comparison test: *: $p < 0.05$. Control: w; *sns*-Gal4/+;UAS-*dicer2*/+. Piezo WT: w; *sns*-Gal4/+;UAS-*dicer2*/UAS-*piezo*-flag. Piezo w/o MS: w; *sns*-Gal4/+;UAS-*GCaMP6m*/UAS-*piezo*-2306MYC.flag. **B** Immunofluorescence staining to visualize the nephrocyte diaphragm at 28°C (high expression levels)

368 also reveal a severe and significant phenotype upon expression of Piezo wildtype, while pericardial cells
369 expressing the mutant exhibit a normal morphology. Scale bar = 5μm. 1way-ANOVA with Tukey's
370 multiple comparison test: *: $p < 0.05$. **C,D** FITC-Albumin uptake assays reveal a severe phenotype in
371 adult pericardial cells overexpressing wildtype Piezo at 25°C (medium levels) and 28°C (high levels).
372 Expression of the mutant variant of Piezo does not reveal a functional defect, neither at 25°C nor at
373 28°C. Scale bar = 25μm. 1way-ANOVA with Tukey's multiple comparison test: **: $p < 0.01$; ***: $p <$
374 0.001. **E** Visualization of actin fibres by phalloidin immunofluorescence reveals a significant increase of
375 cortical actin fibres in Piezo wildtype overexpressing adult pericardial cells, while surface levels are not
376 altered. Scale bar = 25μm. Student's t-test: *: $p < 0.05$.
377

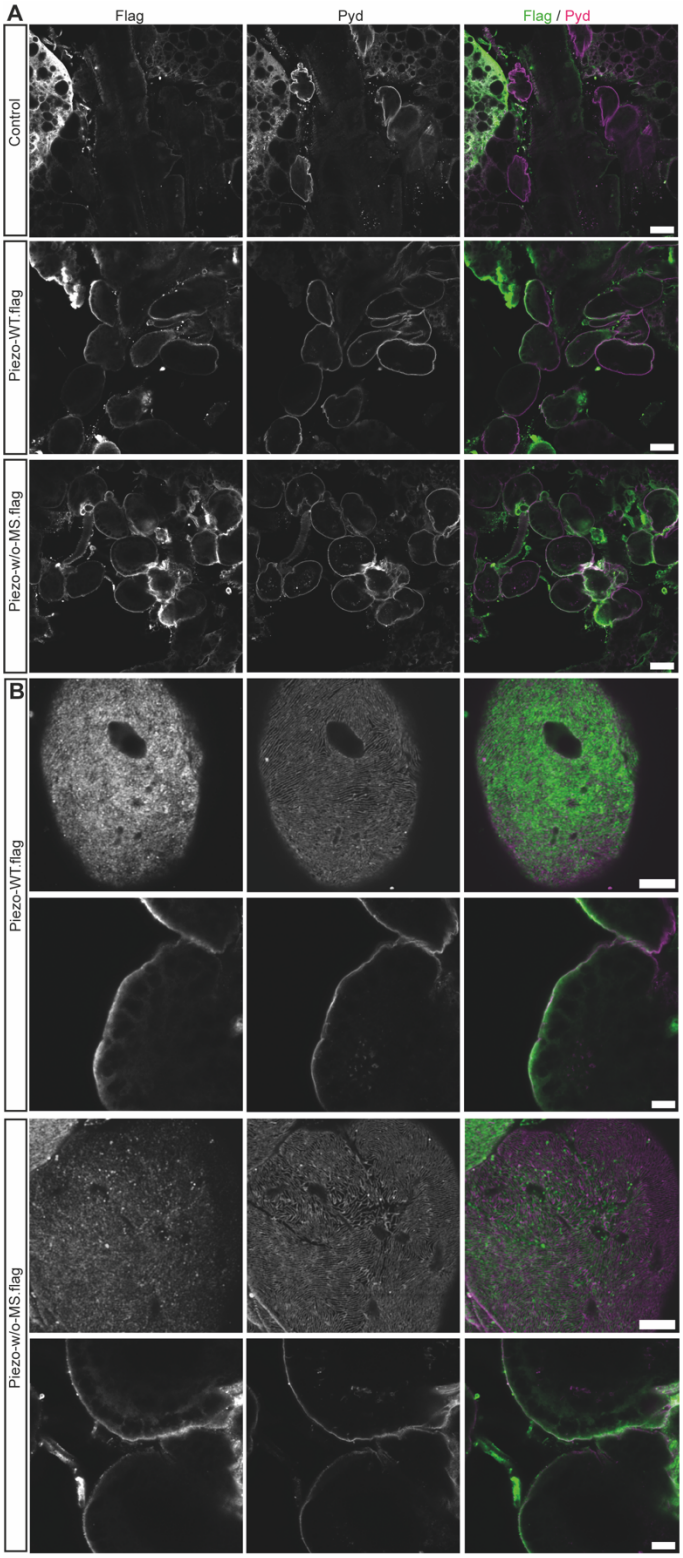

Supp. Fig. 2

Supp. Figure 2: Overexpression of Piezo wildtype and a Piezo mutant lacking the mechanosensitive domain. A Immunofluoresence of adult pericardial nephrocytes expressing Piezo wildtype or the mutant Piezo at 25°C visualizing the nephrocyte diaphragm with a Pyd antibody and the flag tag to visualize Piezo. Scale bar = 25μm (upper three rows) and 5μm. Control: w; *sns*-Gal4/+;UAS-*dicer2*/+. Piezo WT: w; *sns*-Gal4/+;UAS-*dicer2*/UAS-*piezo*-flag. Piezo w/o MS: w; *sns*-Gal4/+;UAS-*GCaMP6m*/UAS-*piezo*-2306MYC.flag.

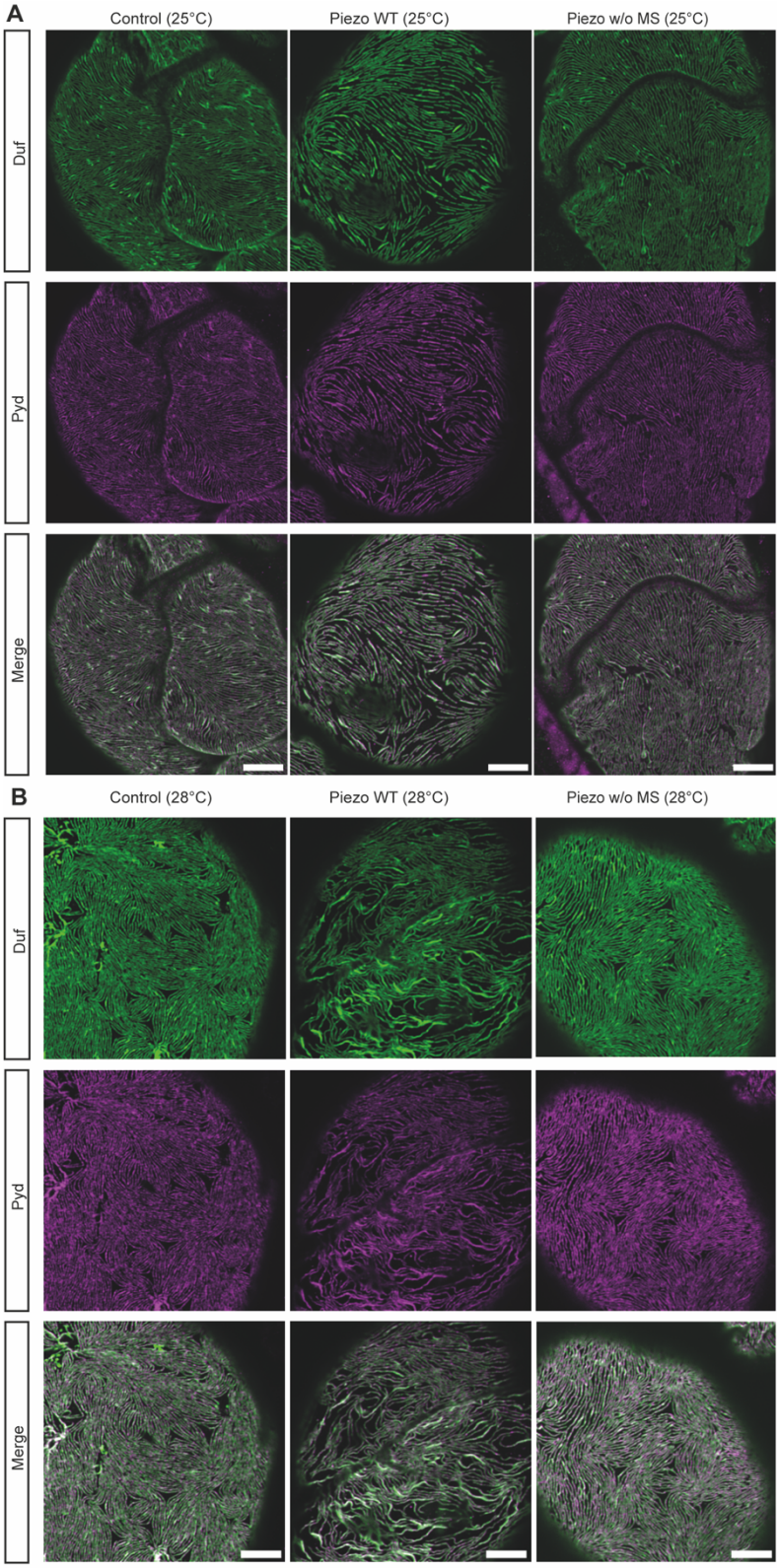

Supp. Fig. 3

Supp. Figure 3: Overexpression of Piezo causes a nephrocyte phenotype, which is mediated by the mechanosensitive channel domain. A,B Immunofluoresence of adult pericardial nephrocytes expressing Piezo wildtype or the mutant Piezo at 25°C (medium levels) and 28°C (high levels) visualizing the nephrocyte diaphragm with Duf and Pyd antibodies. Scale bar = 5μm. Control: w; *sns*-Gal4/+;UAS-*dicer2*/+. Piezo WT: w; *sns*-Gal4/+;UAS-*dicer2*/UAS-*piezo*-flag. Piezo w/o MS: w; *sns*-Gal4/+;UAS-*GCaMP6m*/UAS-*piezo*-2306MYC.flag.

393 **Pharmacological inhibition with tarantula toxin reverses the nephrocyte**
394 **phenotypes observed upon overexpression of Piezo**

395 Overexpression of Piezo has a detrimental effect on nephrocyte biology. Therefore,
396 we tested whether pharmacological inhibition of the channel could reverse the
397 phenotypes we observed. To do so, we used tarantula toxin (GsMTx4), which
398 integrates into the cell membrane and blocks the opening of the channel upon
399 mechanical stretch [39] . Of note, GsMTx4 is not specific for inhibiting Piezo, but also
400 acts on other cation channels.

401 First, we assessed whether treatment of pericardial cells with GsMTx4 results
402 in a nephrocyte phenotype. Analysing morphology and function, we did not observe
403 any significant changes in wildtype flies **(Figure 6A,B,C,D).** Next, we investigated
404 whether a 5mins incubation of pericardial nephrocytes with the toxin reverses the
405 morphological phenotype observed upon overexpression of Piezo wildtype. Adult
406 pericardial cells present with a significant rescue of the morphological phenotype after
407 GsMTx4 treatment **(Figure 6A,B; Supp. Figure 4)**. Moreover, FITC-Albumin uptake
408 assays also reveal a significant rescue of the functional defect induced by Piezo
409 overexpression after GsMTx4 treatment **(Figure 6C,D)**.

410 Taken together, a treatment with the toxin did not reveal pathological effects on
411 nephrocyte morphology and function, but reversed the phenotypes observed in
412 nephrocytes overexpressing Piezo wildtype and might therefore be a potential
413 intervention to prevent Piezo associated phenotypes.

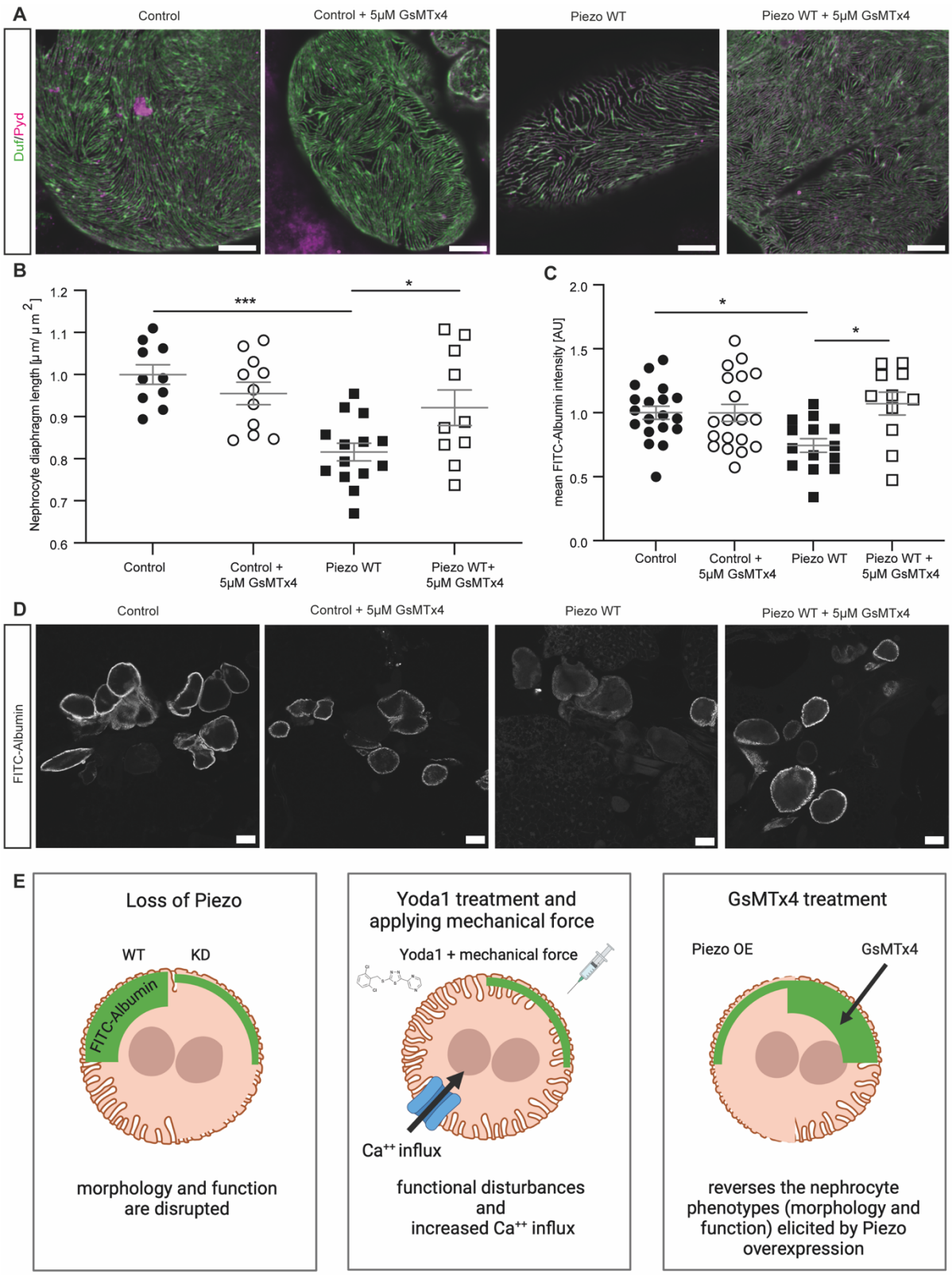

Figure 6

Figure 6: GsMTx4 treatment reverses the phenotypes observed in nephrocytes overexpressing Piezo wildtype. A,B Immunofluorescence staining with Duf and Pyd antibodies reveals a rescue of the morphological changes in adult pericardial cells expressing Piezo wildtype after incubation with 5µM GsMTx4 for 5mins. 1way-ANOVA with Tukey's multiple comparison test: *: $p < 0.05$; ***: $p < 0.001$. Control: w; *sns*-Gal4/+;UAS-*dicer2*/+. Piezo WT: w; *sns*-Gal4/+;UAS-*dicer2*/UAS-*piezo*-flag. **C,D** FITC-Albumin uptake assays show a rescue of the observed phenotype in adult pericardial nephrocytes

overexpressing Piezo wildtype after 5mins GsMTx4 treatment. 1way-ANOVA with Tukey's multiple comparison test: *: $p < 0.05$. **E** Schematic summarising the data. First panel: Loss of Piezo causes a morphological and functional phenotype, which is most severe in adult pericardial cells at 28°C. Second panel: Pharmacological activation of endogenous Piezo by Yoda1 treatment and applying mechanical force causes functional defects and increased Ca^{++} influx. Third panel: Overexpression of wildtype Piezo in adult pericardial nephrocytes results in morphological and functional disturbances. These phenotypes seem to be mediated by the mechanosensitive channel activity of Piezo. Treatment of Piezo wildtype overexpressing nephrocytes with GsMTx4 reversed the observed phenotypes. All images have been created with BioRender.com.

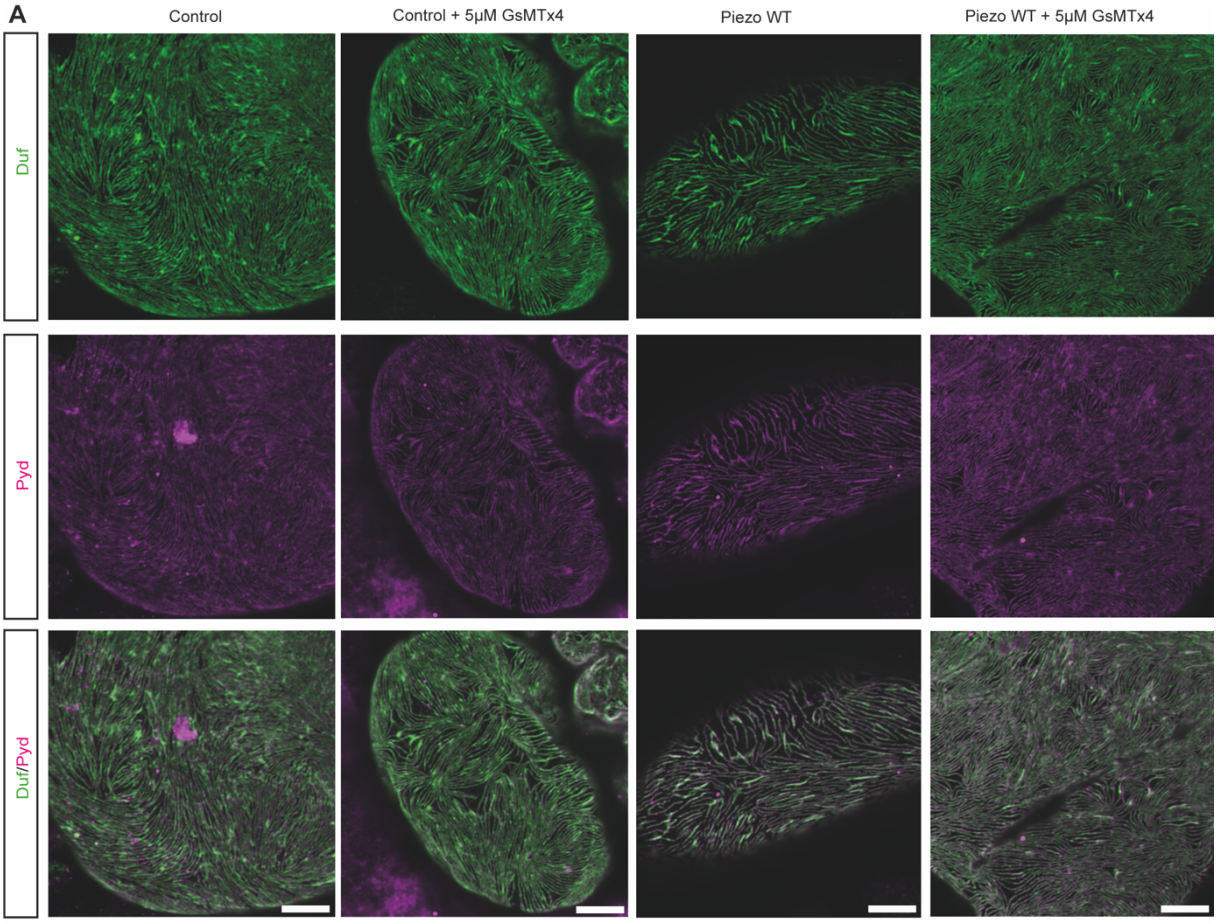

Supp. Figure 4

Supp. Figure 4: GsMTx4 treatment reverses the morphological phenotype observed in adult pericardial nephrocytes overexpressing Piezo wildtype. A Immunofluorescence staining with Duf and Pyd antibodies reveals a rescue of the morphological changes after incubation with 5µM GsMTx4 for 5mins in adult pericardial cells expressing Piezo wildtype. Scale bar = 5µm. Control: w; *sns*-Gal4/+;UAS-*dicer2*/+. Piezo WT: w; *sns*-Gal4/+;UAS-*dicer2*/UAS-*piezo*-flag.

442 **Discussion**

443 Mechanotransducers play a crucial role in podocyte biology and within this
444 study, we describe the role of the mechanosensitive ion channel Piezo in Drosophila
445 nephrocytes **(Figure 6E)**. Here, we could show expression of Piezo1 in murine
446 podocytes by immunofluorescence, localizing within foot processes and the cell body.
447 This confirms RNAscope data showing Piezo1 expression in podocytes from a recently
448 published study [32]. The authors also report an upregulation of Piezo1 in their
449 experimental hypertensive nephropathy model in podocytes [32], illustrating the need to
450 investigate both, loss and overexpression of the channel, to characterize its functional
451 role. Another recent publication could also show expression of Piezo1 in podocytes
452 and an increase of Piezo1 in podocytes in lupus nephritis [33]. Our data shows that both,
453 depletion and overexpression of wildtype Piezo result in a severe pericardial
454 nephrocyte phenotype. This includes morphological alterations of the nephrocyte
455 diaphragm, which results in a less dense expression pattern of Duf (dNEPH) and Pyd
456 (dZO1), and functional disturbances, as assessed by FITC-Albumin uptake assays. To
457 understand the functional role of the Piezo protein in nephrocytes in greater detail, we
458 also investigated a mutant fly strain lacking the mechanosensitive channel activity.
459 Interestingly, this mutant does not present with a pericardial nephrocyte phenotype.
460 Even after increasing expression levels further, morphology or function are not
461 changed, suggesting that the observed phenotype is at least partially mediated via the
462 mechanosensitive domain.

463 In addition to depletion and overexpression, we aimed to unravel the effects of
464 activating endogenous Piezo in the presence of mechanical force. To do so, we used
465 Yoda1 to pharmacologically activate endogenous Piezo. Here, we could show a
466 filtration defect after Yoda1 treatment and applying a mechanical stimulus. This
467 confirms our hypothesis of Piezo expression in nephrocytes and its importance in

468 nephrocyte biology. We further confirmed this hypothesis by performing all Yoda1
469 experiments in a Piezo knockdown background, which abrogates the observed
470 filtration defect.

471 Within this study, we also performed Ca^{++} imaging in isolated pericardial cells
472 from adult flies and could show an increase of intracellular Ca^{++} levels after applying
473 mechanical stimuli and pretreatment with Yoda1. This elevated Ca^{++} influx was
474 abrogated by depleting Piezo in nephrocytes, confirming that the influx is at least
475 partially mediated via Piezo. Our data suggests an opening of the channel upon a
476 mechanical stimulus (puff) in nephrocytes, which is facilitated after binding of Yoda1
477 between the Arm domain and the repeat A [36]. In a recent study, Sivakumar et al.
478 showed that nephrocytes exhibit spontaneous calcium signals *in vivo* [37], which was
479 also observed here. Analysing peak amplitude parameters enabled us to distinguish
480 between the spontaneous calcium signals and the signals elicited after applying a puff.
481 Sivakumar et al. were also able to show a functional role of store operated Ca^{++} entry
482 (SOCE) mechanisms, in particular Stim and Orai-dependent, on nephrocyte
483 endocytosis [37]. Thus, this data, together with the data provided in here, show that Ca^{++}
484 signalling is an important signalling feature in *Drosophila* nephrocytes.

485 Of note, in about half of the flies in our study (treated either with DMSO or
486 Yoda1), Ca^{++} levels did not return to baseline levels within the timeframe of the
487 recordings. This data suggests, that the mechanical stimulus applied, modulates
488 several different Ca^{++} transport (import and export) mechanisms (e.g. SOCE), which
489 slow down the decrease of intracellular Ca^{++} levels.

490 Mechanosensors, such as TRP channels, have also been described to regulate
491 GTPase activation in podocytes [40]. One downstream target of GTPases and Ca^{++}
492 signalling is the actin cytoskeleton, which plays an essential role during podocyte injury
493 and rearrangement processes [41]. A previous study described actin clusters and cortical

494 actin in nephrocytes as well [42]. Here, we also assessed the actin cytoskeleton after
495 Yoda1 treatment and applying mechanical force as well as upon overexpression of
496 Piezo wildtype. While activation of endogenous Piezo does not result in alterations of
497 the actin cytoskeleton, overexpression of Piezo caused an increase of cortical actin
498 fibres. In *in vitro* podocytes activation of Piezo also caused actin cytoskeleton
499 remodelling as a result of Rac1 activation [33]. Of note, the absence of a phenotype upon
500 Yoda1 treatment and applying mechanical force in our experiment, might be explained
501 by the time frame of the experiment. Longer exposure of Yoda1, for example by
502 feeding, is very interesting, but beyond the scope of this study. However, the more
503 artificial condition of overexpression of Piezo, suggests an impact on the actin
504 cytoskeleton, which might be mediated by alterations in Ca^{++} influx, in nephrocytes.

505 Our findings, that actin fibre formation might have relevance to nephrocytes
506 response to injury, are supported by a previous study investigating the effect of Bis-T-
507 23 in podocytes. Bis-T-23 promotes actin-dependent dynamin oligomerization and
508 stabilizes the actin cytoskeleton during podocyte injury [43]. In detail, several injury
509 models which caused actin-cytoskeleton rearrangement could be at least partially
510 rescued by Bis-T-23 treatment, again emphasising the importance of the actin-
511 cytoskeleton and upstream regulators such as GTPases [43].

512 Analysing publicly available data from the Kidney Precision Medicine Project
513 (KPMP) revealed an increase of Piezo1 in podocytes in CKD samples, which is in line
514 with data obtained from experimental hypertensive nephropathy and lupus nephritis
515 mouse models [32,33]. Hence, a treatment to block Piezo activation could be beneficial
516 for patients. Our data showed that the treatment with tarantula toxin (GsMTx4) was
517 able to, reverse the observed phenotypes in nephrocytes overexpressing Piezo
518 wildtype. This is in line with data showing improved kidney function in a lupus mouse
519 model after GsMTx4 treatment [33]. In addition, another study investigated the

520 association between Piezo1 activation and kidney fibrosis [44]. Tubular Piezo1 was
521 increased in fibrotic kidneys and inhibition of Piezo1 with GsMTx4 resulted in
522 attenuated tubulointerstitial fibrosis [44], further supporting the idea of GsMTx4 use as a
523 potential intervention in the future. However, we want to mention that GsMTx4 is not
524 specific to Piezo, but also inhibits other mechanosensitive channels. Interestingly,
525 Piezo2 has recently been described to be expressed in renin-producing cells of the
526 juxta-glomerular apparatus and mesangial cells in the kidney, where it contributes to
527 renal blood volume sensing [45,46].

528 Taken together, here we provide evidence that the mechanosensitive ion
529 channel Piezo is expressed in podocytes and nephrocytes and that Piezo activity levels
530 need to be tightly regulated in order to maintain normal morphology and function in
531 adult pericardial nephrocytes.

532
533
534
535
536
537
538
539
540
541
542
543
544
545

546 **Methods**

547 **Tables**

548 **Table 1: List of fly strains**

Fly strain	Origin	Purpose	Chromosome
UAS-*piezo*-flag	BDSC ID: 95296	Overexpression	3. Chr.
UAS-*piezo*.2306MYC.flag	BDSC ID: 95298	Overexpression	3. Chr.
UAS-*piezo*-RNAi	VDRC ID: 101915	Knockdown	2. Chr.
sns-Gal4; UAS-*dicer*2	the *sns*-Gal4 strain was obtained from S. Abmayr [47] and combined with UAS-*dicer2* [8]	Nephrocyte-specific driver	2. + 3. Chr.
UAS-GCaMP6medium	BDSC ID: 42750	Overexpression	3. Chr.
W^{1118}		wildtype	

549

550 **Table 2: List of antibodies**

Name	Company/ Provider	Catalog nr. / Reference	Host Species	Dilution IF
Duf	M. Ruiz-Gomez	[28]	Rabbit	1:100
Pyd	Developmental Studies Hybridoma Bank	PYD2	Mouse	1:25

Piezo1	Proteintech	28511-1-AP	Rabbit	1:100
Synaptopodin	Synaptic Systems	163 004	Guinea Pig	1:200

551
552

553 **Fly husbandry**

554 The UAS-Gal4 system is influenced by temperature, being more active at a higher
555 temperature, thus we used two different temperatures (medium: 25°C and high: 28°C)
556 for our experiments. The nephrocyte-specific knockdown or overexpression was
557 achieved by mating UAS fly strains with the *sns*-Gal4 strain. Fly strains are listed in
558 **table 1**.

559

560 **Yoda1 and GsMTx4 treatment**

561 To activate Piezo, nephrocytes were incubated with the specific activator compound
562 Yoda1 for 5mins (30μM in DMSO; control: DMSO) (Sigma, now Merck). A mechanical
563 stimulus was applied using the pressure injector SYS-PV830 (W.P.I. Instruments,
564 Friedberg, Germany) in combination with a 1ml syringe fitted with a 26G needle as
565 applicator nozzle. The syringe was either filled with Yoda1 (30μM) or DMSO (equal
566 amount to Yoda1) and positioned with the same angle and position relative to the bath
567 solution's surface throughout the experiments. The tissue was incubated in the
568 respective bath solution for 5mins prior to applying the mechanical stimulus. This was
569 achieved by pressure-controlled release of the syringe solution (referred to as a puff,
570 0.2bar for 3secs) to simulate the induction of shear stress. To inhibit mechanosensitive
571 channel activity, nephrocytes were incubated with the unspecific cationic

572 mechanosensitive channel inhibitor tarantula toxin/GsMTx4 for 5mins (5μM in H_2O;
573 control: HL3.1 buffer) (Alomone labs, Jerusalem, Israel, Cat. nr: STG-100).
574
575 **Immunofluorescences of *Drosophila* tissue**
576 Garland nephrocytes were isolated from 3rd instar larvae in HL3.1 buffer. For isolation
577 of pericardial cells, the cuticle of the abdomen of 1-3 days old flies were dissected
578 leaving pericardial cells still attached to the heart tube. The whole tissue was used for
579 immunofluorescence staining and the dissection was performed in HL3.1 buffer. After
580 isolation, cells were fixed in 4% formaldehyde for 20mins and one hour in methanol.
581 Primary and secondary antibody (see **table 2**) incubation was done according to
582 standard procedures overnight at 4°C. Imaging was done using either a Zeiss LSM
583 800 confocal combined with an Airyscan for higher resolution or a Leica SP8 confocal.
584 Images were further processed using ImageJ (version 1.53c). To quantify nephrocyte
585 density (nephrocyte diaphragm length [$\mu m/\mu m^2$]) we used our previously published
586 macro for FIJI, which was adapted for Airyscan confocal images [48].
587
588 **Immunofluorescence of murine tissue**
589 Paraffin-embedded tissue from wildtype mice was used for immunofluorescence
590 staining. Tissue was de-paraffinized by passing through a descending alcohol row.
591 After washing for three times (5 mins) with H_2O followed by three washing steps with
592 Dako wash buffer (Agilent Technologies, Santa Clara, USA), antigen retrieval was
593 done in a steamer using pH9 antigen retrieval from Dako. Primary antibodies (listed in
594 Table 1) were diluted in Dako antibody diluent and incubated overnight at 4°C. The
595 next day sections were washed for three times (5 mins) with Dako wash buffer,
596 followed by secondary antibody incubation with DAPI for one hour at room
597 temperature. Prior to mounting with Prolong Gold, samples were again washed three

598 times. Imaging of samples was done at a Zeiss LSM 900 confocal combined with
599 Airyscan. Images were further processed using ImageJ (version 1.53c).
600
601 **FITC-Albumin uptake assay**
602 FITC-Albumin uptake assays were performed as previously published [8,49]. Uptake of
603 FITC-Albumin into the lacunae is a read-out for nephrocyte function. Pericardial cells
604 were isolated from 1-3 days old adults. Imaging was done with a Zeiss LSM 5 confocal,
605 a Leica SP8 confocal and a Zeiss LSM 800 confocal microscope and images were
606 further processed and analysed using ImageJ (version 1.53c). For comparative
607 analysis, the exposure time of experiments was kept identical. The mean intensity of
608 FITC-Albumin was measured and normalized to control cells.
609
610 **Visualization and quantification of actin fibres**
611 To visualize actin fibres, we used phalloidin. For actin quantification cortical and
612 surface mean intensities of phalloidin were measured. Images were obtained using a
613 Zeiss LSM800 confocal microscope combined with Airyscan and further image
614 processing was done using ImageJ (version 1.53c). For comparative analysis, laser
615 intensity and settings were kept equal. Quantification of cortical fibres was done using
616 the brush selection tool from FIJI.
617
618 **Ca^{++} imaging of pericardial nephrocytes**
619 For Ca^{++} imaging experiments, UAS-GCaMP6m flies were combined with the
620 nephrocyte-driver *sns*-Gal4 to obtain experimental animals. Flies were kept at 25°C
621 until the experimental flies were 1-3 days old. Flies were anesthetized with Flynap
622 (Carolina Biological Supply company, North Carolina, USA). Pericardial nephrocytes
623 were isolated but still attached to the heart tube and the cuticle. The tissue was glued

624 onto coverslips with vaseline and transferred into a recording chamber. The
625 experimental setup was consistent with the previously described experiments (Yoda1
626 treatment). The recording bath was filled with either 1ml Yoda1 (30µM) in HL3.1 buffer
627 or an equivalent volume of DMSO in HL3.1 buffer. The tissue was incubated in the
628 respective bath solution for 5mins before applying a pressure stimulus. Using the same
629 method as before, a 1ml syringe with a 26G needle, filled with either Yoda1 (30µM) or
630 DMSO, was positioned on the surface of the bath solution and the syringe solution was
631 released as a puff (0.2bar for 3secs, PDES-01 a.m., NPI Electronic GmbH, Tamm,
632 Germany) to simulate shear stress. GCaMP6 was excited at 488nm, and fluorescence
633 was collected between 500 and 530nm using a confocal microscope (eC1, Nikon,
634 Düsseldorf, Germany). Time series of images were recorded at a rate of 1.26 frame
635 per second. Data was evaluated with Nikon EZ-C1 Viewer (Nikon), processed using
636 Excel (Microsoft, USA), and statistical tests were applied with Graph Pad Prism
637 software. GCaMP6m-expressing nephrocytes were marked as a region of interest
638 (ROI) and the mean fluorescence intensity within the ROI was measured throughout
639 the time series. The mean fluorescence intensity (F) was normalized to the baseline
640 fluorescence intensity before the puff (mean of 10 values prior to puff) and set to 1.0,
641 hence changes in fluorescence intensity are stated as ΔF. Quantification of Ca^{++}
642 transients (peak amplitude) was achieved by calculating the maximum increase of
643 GCaMP6 intensity after the puff within 25secs after puff. The number of experiments
644 is given as n, where n represents the averaged values of all ROIs analysed in one fly
645 and equals one datapoint in the graphs. The figure legends include a depiction of how
646 many flies and ROIs per condition were investigated. Traces of calcium signals were
647 created with OriginPro 9.1G (OriginLab Corporation, USA) and composed using Adobe
648 Illustrator and Adobe Photoshop (Adobe Systems Software, Ireland). Visualizations of
649 changes in fluorescence were created using Fiji ImageJ (National Institutes of Health,

650 USA) and composed with Adobe Photoshop (Adobe Systems Software, Ireland). In
651 these visualizations, red signals indicate the difference between baseline brightness
652 and brightness at the indicated timeslots (ΔF), the grey background signal represents
653 baseline fluorescence prior to applied stimuli.
654
655 **Transcriptomic data analysis**
656 Publicly available human single nucleus RNA-sequencing (snRNAseq) [34] data were
657 searched for Piezo1 expression. Data and analyser have been used provided by KIT
658 (kidney interactive transcriptomics) http://humphreyslab.com/SingleCell/. Permission
659 to use the graphs generated has been provided by Benjamin Humphreys. In addition,
660 human single cell RNA-sequencing data (scRNAseq) provided by the Kidney Precision
661 Medicine Project (KPMP) consortium were searched for Piezo1 expression. The
662 results here are in whole or part based upon data generated by the Kidney Precision
663 Medicine Project. Accessed November 14th, 2023. https://www.kpmp.org. Funded by
664 the National Institute of Diabetes and Digestive and Kidney Diseases (Grant numbers:
665 U01DK133081, U01DK133091, U01DK133092, U01DK133093, U01DK133095,
666 U01DK133097, U01DK114866, U01DK114908, U01DK133090, U01DK133113,
667 U01DK133766, U01DK133768, U01DK114907, U01DK114920, U01DK114923,
668 U01DK114933, U24DK114886, UH3DK114926, UH3DK114861, UH3DK114915,
669 UH3DK114937).
670
671 **Statistical analysis**
672 To determine statistical significance Graph Pad Prism software version 8 for Mac
673 (GraphPad Software, San Diego, CA) was used. All results are expressed as means
674 ± SEM. Datapoints represent single flies from 2 to 3 independent matings. Mean values
675 from all imaged nephrocytes of one fly have been calculated and are shown as one

676 datapoint in the graphs. Comparison of two groups was done using a student's t-test,
677 while comparison of more than two groups with one independent variable was done
678 using one-way ANOVA followed by Tukey's multiple comparisons test. A *P-value* <
679 0.05 was considered statistically significant.

680

681 **References**

682 1. Pavenstädt H, Kriz W, Kretzler M: Cell biology of the glomerular podocyte. *Physiol.*
683 *Rev.* 83: 253–307, 2003
684 2. Kestilä M, Lenkkeri U, Männikkö M, Lamerdin J, McCready P, Putaala H, et al.:
685 Positionally cloned gene for a novel glomerular protein--nephrin--is mutated in congenital
686 nephrotic syndrome. *Mol. Cell* 1: 575–582, 1998
687 3. Boute N, Gribouval O, Roselli S, Benessy F, Lee H, Fuchshuber A, et al.: NPHS2,
688 encoding the glomerular protein podocin, is mutated in autosomal recessive steroid-resistant
689 nephrotic syndrome. *Nat. Genet.* 24: 349–354, 2000
690 4. Kaplan JM, Kim SH, North KN, Rennke H, Correia LA, Tong HQ, et al.: Mutations in
691 ACTN4, encoding alpha-actinin-4, cause familial focal segmental glomerulosclerosis. *Nat.*
692 *Genet.* 24: 251–256, 2000
693 5. Winn MP, Conlon PJ, Lynn KL, Farrington MK, Creazzo T, Hawkins AF, et al.: A
694 mutation in the TRPC6 cation channel causes familial focal segmental glomerulosclerosis.
695 *Science* 308: 1801–1804, 2005
696 6. Hildebrandt F: Genetic kidney diseases. *Lancet Lond. Engl.* 375: 1287–1295, 2010
697 7. Markowitz GS, Bomback AS, Perazella MA: Drug-Induced Glomerular Disease:
698 Direct Cellular Injury. *Clin. J. Am. Soc. Nephrol.* 10: 1291–1299, 2015
699 8. Koehler S, Kuczkowski A, Kuehne L, Jüngst C, Hoehne M, Grahammer F, et al.:
700 Proteome Analysis of Isolated Podocytes Reveals Stress Responses in Glomerular Sclerosis.
701 *J. Am. Soc. Nephrol. JASN* 31: 544–559, 2020
702 9. Greiten JK, Kliewe F, Schnarre A, Artelt N, Schröder S, Rogge H, et al.: The role of
703 filamins in mechanically stressed podocytes. *FASEB J. Off. Publ. Fed. Am. Soc. Exp. Biol.* 35:
704 e21560, 2021
705 10. Feng D, DuMontier C, Pollak MR: Mechanical challenges and cytoskeletal
706 impairments in focal segmental glomerulosclerosis. *Am. J. Physiol. - Ren. Physiol.* 314:
707 F921–F925, 2018
708 11. Endlich N, Kress KR, Reiser J, Uttenweiler D, Kriz W, Mundel P, et al.: Podocytes
709 respond to mechanical stress in vitro. *J. Am. Soc. Nephrol. JASN* 12: 413–422, 2001
710 12. Endlich K, Kliewe F, Endlich N: Stressed podocytes-mechanical forces, sensors,
711 signaling and response. *Pflugers Arch.* 469: 937–949, 2017
712 13. Puelles VG, Cullen-McEwen LA, Taylor GE, Li J, Hughson MD, Kerr PG, et al.:
713 Human podocyte depletion in association with older age and hypertension. *Am. J. Physiol.-*
714 *Ren. Physiol.* 310: F656–F668, 2016
715 14. Kriz W, Lemley KV: Mechanical challenges to the glomerular filtration barrier:
716 adaptations and pathway to sclerosis. *Pediatr. Nephrol.* 32: 405–417, 2017
717 15. Haley KE, Kronenberg NM, Liehm P, Elshani M, Bell C, Harrison DJ, et al.: Podocyte
718 injury elicits loss and recovery of cellular forces. *Sci. Adv.* 4: eaap8030, 2018
719 16. Kriz W, Lemley KV: A Potential Role for Mechanical Forces in the Detachment of
720 Podocytes and the Progression of CKD. *J. Am. Soc. Nephrol.* 26: 258–269, 2015

721 17. Wiggins JE, Goyal M, Sanden SK, Wharram BL, Shedden KA, Misek DE, et al.:
722 Podocyte hypertrophy, "adaptation," and "decompensation" associated with glomerular
723 enlargement and glomerulosclerosis in the aging rat: prevention by calorie restriction. *J. Am.*
724 *Soc. Nephrol. JASN* 16: 2953–2966, 2005
725 18. Rinschen MM, Grahammer F, Hoppe A-K, Kohli P, Hagmann H, Kretz O, et al.:
726 YAP-mediated mechanotransduction determines the podocyte's response to damage. *Sci.*
727 *Signal.* 10: 2017
728 19. Tian X, Kim JJ, Monkley SM, Gotoh N, Nandez R, Soda K, et al.: Podocyte-
729 associated talin1 is critical for glomerular filtration barrier maintenance. *J. Clin. Invest.* 124:
730 1098–1113, 2014
731 20. Okabe M, Yamamoto K, Miyazaki Y, Motojima M, Ohtsuka M, Pastan I, et al.:
732 Indirect podocyte injury manifested in a partial podocytectomy mouse model. *Am. J. Physiol.*
733 *Renal Physiol.* 2021
734 21. Dalghi MG, Clayton DR, Ruiz WG, Al-bataineh MM, Satlin LM, Kleyman TR, et al.:
735 Expression and distribution of PIEZO1 in the mouse urinary tract. *Am. J. Physiol.-Ren.*
736 *Physiol.* 317: F303–F321, 2019
737 22. Coste B, Mathur J, Schmidt M, Earley TJ, Ranade S, Petrus MJ, et al.: Piezo1 and
738 Piezo2 are essential components of distinct mechanically activated cation channels. *Science*
739 330: 55–60, 2010
740 23. Coste B, Xiao B, Santos JS, Syeda R, Grandl J, Spencer KS, et al.: Piezo proteins are
741 pore-forming subunits of mechanically activated channels. *Nature* 483: 176–181, 2012
742 24. Cahalan SM, Lukacs V, Ranade SS, Chien S, Bandell M, Patapoutian A: Piezo1 links
743 mechanical forces to red blood cell volume. *eLife* 4: 2015
744 25. Ranade SS, Qiu Z, Woo S-H, Hur SS, Murthy SE, Cahalan SM, et al.: Piezo1, a
745 mechanically activated ion channel, is required for vascular development in mice. *Proc. Natl.*
746 *Acad. Sci. U. S. A.* 111: 10347–10352, 2014
747 26. Retailleau K, Duprat F, Arhatte M, Ranade SS, Peyronnet R, Martins JR, et al.: Piezo1
748 in Smooth Muscle Cells Is Involved in Hypertension-Dependent Arterial Remodeling. *Cell*
749 *Rep.* 13: 1161–1171, 2015
750 27. Zhong M, Komarova Y, Rehman J, Malik AB: Mechanosensing Piezo channels in
751 tissue homeostasis including their role in lungs. *Pulm. Circ.* 8: 2045894018767393, 2018
752 28. Weavers H, Prieto-Sánchez S, Grawe F, Garcia-López A, Artero R, Wilsch-
753 Bräuninger M, et al.: The insect nephrocyte is a podocyte-like cell with a filtration slit
754 diaphragm. *Nature* 457: 322–326, 2009
755 29. Zhuang S, Shao H, Guo F, Trimble R, Pearce E, Abmayr SM: Sns and Kirre, the
756 Drosophila orthologs of Nephrin and Neph1, direct adhesion, fusion and formation of a slit
757 diaphragm-like structure in insect nephrocytes. *Dev. Camb. Engl.* 136: 2335–2344, 2009
758 30. Xu J, Liu Y, Li H, Tarashansky AJ, Kalicki CH, Hung R-J, et al.: Transcriptional and
759 functional motifs defining renal function revealed by single-nucleus RNA sequencing. *Proc.*
760 *Natl. Acad. Sci.* 119: e2203179119, 2022
761 31. Rinschen MM, Gödel M, Grahammer F, Zschiedrich S, Helmstädter M, Kretz O, et
762 al.: A Multi-layered Quantitative In Vivo Expression Atlas of the Podocyte Unravels Kidney
763 Disease Candidate Genes. *Cell Rep.* 23: 2495–2508, 2018
764 32. Ogino S, Yoshikawa K, Nagase T, Mikami K, Nagase M: Roles of the
765 mechanosensitive ion channel Piezo1 in the renal podocyte injury of experimental
766 hypertensive nephropathy. *Hypertens. Res.* 47: 747–759, 2024
767 33. Fu R, Wang W, Huo Y, Li L, Chen R, Lin Z, et al.: The mechanosensitive ion channel
768 Piezo1 contributes to podocyte cytoskeleton remodeling and development of proteinuria in
769 lupus nephritis. *Kidney Int.* S0085253824005295, 2024
770 34. Wilson PC, Muto Y, Wu H, Karihaloo A, Waikar SS, Humphreys BD: Multimodal
771 single cell sequencing implicates chromatin accessibility and genetic background in diabetic

kidney disease progression. *Nat. Commun.* 13: 5253, 2022
35. Syeda R, Xu J, Dubin AE, Coste B, Mathur J, Huynh T, et al.: Chemical activation of the mechanotransduction channel Piezo1. *eLife* 4: 2015
36. Botello-Smith WM, Jiang W, Zhang H, Ozkan AD, Lin Y-C, Pham CN, et al.: A mechanism for the activation of the mechanosensitive Piezo1 channel by the small molecule Yoda1. *Nat. Commun.* 10: 4503, 2019
37. Sivakumar S, Miellet S, Clarke C, Hartley PS: Insect nephrocyte function is regulated by a store operated calcium entry mechanism controlling endocytosis and Amnionless turnover. *J. Insect Physiol.* 143: 104453, 2022
38. Xie Q, Li J, Li H, Udeshi ND, Svinkina T, Orlin D, et al.: Transcription factor Acj6 controls dendrite targeting via a combinatorial cell-surface code. *Neuron* 110: 2299-2314.e8, 2022
39. Suchyna TM, Johnson JH, Hamer K, Leykam JF, Gage DA, Clemo HF, et al.: Identification of a peptide toxin from Grammostola spatulata spider venom that blocks cation-selective stretch-activated channels. *J. Gen. Physiol.* 115: 583–598, 2000
40. Tian D, Jacobo SMP, Billing D, Rozkalne A, Gage SD, Anagnostou T, et al.: Antagonistic regulation of actin dynamics and cell motility by TRPC5 and TRPC6 channels. *Sci. Signal.* 3: ra77, 2010
41. Wang Q, Tian X, Wang Y, Wang Y, Li J, Zhao T, et al.: Role of Transient Receptor Potential Canonical Channel 6 (TRPC6) in Diabetic Kidney Disease by Regulating Podocyte Actin Cytoskeleton Rearrangement. *J. Diabetes Res.* [Internet] 2020: 2020 Available from: https://www.ncbi.nlm.nih.gov/pmc/articles/PMC6964719/ [cited 2021 Jun 15]
42. Muraleedharan S, Sam A, Skaer H, Inamdar MS: Networks that link cytoskeletal regulators and diaphragm proteins underpin filtration function in Drosophila nephrocytes. *Exp. Cell Res.* 364: 234–242, 2018
43. Schiffer M, Teng B, Gu C, Shchedrina VA, Kasaikina M, Pham VA, et al.: Pharmacological targeting of actin-dependent dynamin oligomerization ameliorates chronic kidney disease in diverse animal models. *Nat. Med.* 21: 601–609, 2015
44. Zhao X, Kong Y, Liang B, Xu J, Lin Y, Zhou N, et al.: Mechanosensitive Piezo1 channels mediate renal fibrosis. *JCI Insight* 7: e152330, 2022
45. Hill RZ, Shirvan S, Burquez S, Dubin AE, Servin-Vences MR, Miner JH, et al.: Renal mechanotransduction is an essential regulator of renin [Internet]. Physiology; Available from: http://biorxiv.org/lookup/doi/10.1101/2023.11.04.565646 [cited 2023 Nov 14]
46. Liu S, Zhao Y, Lu S, Zhang T, Lindenmeyer MT, Nair V, et al.: Single-cell transcriptomics reveals a mechanosensitive injury signaling pathway in early diabetic nephropathy. *Genome Med.* 15: 2, 2023
47. Kocherlakota KS, Wu J, McDermott J, Abmayr SM: Analysis of the Cell Adhesion Molecule Sticks-and-Stones Reveals Multiple Redundant Functional Domains, Protein-Interaction Motifs and Phosphorylated Tyrosines That Direct Myoblast Fusion in *Drosophila melanogaster*. *Genetics* 178: 1371–1383, 2008
48. Koehler S, Odenthal J, Ludwig V, Jess DU, Höhne M, Jüngst C, et al.: Scaffold polarity proteins Par3A and Par3B share redundant functions while Par3B acts independent of atypical protein kinase C/Par6 in podocytes to maintain the kidney filtration barrier. *Kidney Int.* S0085-2538(21)01150–9, 2021
49. Hermle T, Braun DA, Helmstädter M, Huber TB, Hildebrandt F: Modeling Monogenic Human Nephrotic Syndrome in the Drosophila Garland Cell Nephrocyte. *J. Am. Soc. Nephrol. JASN* 28: 1521–1533, 2017
50. Choi W, Jung K-C, Nelson KS, Bhat MA, Beitel GJ, Peifer M, et al.: The single Drosophila ZO-1 protein Polychaetoid regulates embryonic morphogenesis in coordination with Canoe/afadin and Enabled. *Mol. Biol. Cell* 22: 2010–2030, 2011

Acknowledgement

The Anti-Pyd monoclonal antibody developed by Fanning [50] was obtained from the Developmental Studies Hybridoma Bank, created by the NICHD of the NIH and maintained at The University of Iowa, Department of Biology, Iowa City, IA 52242. Images were created with BioRender.com.

Author contribution

S.K. conceived the study, made the figures and wrote the paper, K.S., P.H.-C., K.K.A., I.E. and S.K. performed experiments, S.K., M.L. and K.S. analysed data, B.D., C.L. and T.B.H. revised the study critically for important intellectual content, S.K. and B.D. revised the paper; all authors approved the final version of the manuscript.

Data Availability Statement

Data sharing not applicable as no datasets were generated during this study.

Conflict of Interest Statement

The authors declare no conflicts of interest.

Funding

S.K. received funding from the German Research Foundation (KO 6045/1-1 and KO 6045/4-1) and the Else Kröner Fresenius Foundation (2022_EKEA.09). T.B.H. received funding from the German Research Foundation (CRC1192, HU 1016/8-2, HU 1016/11-1, HU 1016/ 12-1). S.K., M.L. and T.B.H received funding from the BMBF (STOP-FSGS-01GM2202A).